

Directed long-range transport of a nearly pure component atom clusters by the electromigration of a binary surface alloy

Mikhail Khenner^{*1,2}

¹*Department of Mathematics, Western Kentucky University, Bowling Green, KY 42101, USA*

²*Applied Physics Institute, Western Kentucky University, Bowling Green, KY 42101, USA*

(Dated: June 11, 2022)

A continuum model for electromigration-driven transport of an embedded, compact atom cluster across a surface terrace of a phase-separating binary surface alloy is presented. Computations show that the electron wind reliably transports the cluster over hundreds of lattice spacings and in the set direction, while the cluster purity improves during the drift. Impacts on cluster's drift speed and purity of the A to B atom's jump frequencies ratio, the magnitude and the sign of the A and B atoms's effective surface charges, the applied voltage, and the diffusion anisotropy are studied.

Keywords: Surface electromigration; surface alloys; vacancy-mediated diffusion; directed self-assembly; composition patterning.

I. INTRODUCTION

STM studies of the early 2000's [1–3] demonstrated that atoms in close-packed crystal surfaces of pure metals or alloys are highly mobile even at room temperature. For instance, Pd or In atoms incorporated into the topmost layer of Cu(001) substrate may frequently jump over distances larger than one lattice spacing, some as far as five lattice spacings. These jumps are enabled by a fast two-dimensional random walk of vacancies. Of course, the observed two-dimensional motion of impurity atoms reflects the diffusion of all copper atoms in the surface layer. Such vacancy-mediated diffusion of the surface atoms was compared to a giant atomic slide-puzzle [4].

Concerning this phenomenon, the general question one may be asking is this: Is it possible to channel, or bias, the random vacancy-mediated diffusion of individual surface atoms into a collective, directed transport across the surface by the application of the external field or force? In this communication, we answer positively. Using a continuum model based only on the classical diffusion and electromigration phenomenology [5–7], we show that the “electron wind” may transport, over distances of hundreds of lattice spacings and in the set direction on the surface, the compact clusters comprising of, say, predominantly B atom species. As the cluster is transported along the terrace, the persistent phase-separation ensures the continuing in-flow of B atoms and the corresponding out-flow of A atoms from the cluster, until a 100% purity is achieved. The basic necessary conditions are that a phase-separating instability of the surface alloy is activated, and that prior to the onset of the electromigration, there exists a small seed cluster with a spiked concentration of B atoms. Such seed cluster may be artificially created by a local implantation of B atoms into A_xB_{1-x} surface alloy, or it may occur naturally in the said alloy.

The model and the computations are presented in sections II and III, respectively. The model extends the analysis in Ref. [8] and provides a self-consistent formulation, based on irreversible thermodynamics, of the vacancy-mediated embedded atom surface diffusion and electromigration. It is appropriate to remark here that several useful models of surface electromigration-driven nanoisland motion and instabilities were published [9–15], however, these studies do not include alloys and the diffusing and migrating species in this case are the adatoms - thus the diffusion is by the direct exchange of lattice positions.

It is important to point out that the nature of a phase-separating instability is not highly important for the cluster transport on a surface. Any physical mechanism that enhances, in the non-explosive fashion, the initial localized phase inhomogeneity would suffice in the presented model, although the drift speed of the cluster and the (time-dependent) cluster purity will be affected by the detailed workings of the instability. In this communication it is assumed that the surface alloy is thermodynamically unstable, that is, the instability is spinodal [16–18]. This is the simplest phase-separating instability that can be manifested.

We hope that the proposed transport effect of the electric current on the surface atom clusters could be demonstrated in a real-life experiment and then harnessed to enable the localized chemical functionality on metal surfaces, for instance, allow the creation of the mobile catalytic “hot-spot”.

^{*} Corresponding author. E-mail: mikhail.khenner@wku.edu.

II. THE MODEL

We consider a thick conductive film of a uniform composition A, whereby the impurity B atoms are mixed into the topmost surface layer, thus creating a binary surface alloy. The film's surface morphology is comprised of the atomically flat terraces of width L separated by steps. The electric potential difference (voltage) V is applied to the opposite edges of the terrace, which results in the electric field $\mathbf{E} = (E_0 \cos \phi_E, E_0 \sin \phi_E)$, $E_0 = V/L$. Here ϕ_E is the angle that the electric field vector makes with the x -axis of the Cartesian reference frame, see Fig. 1.

Let X_A and X_B be the local time-dependent surface atom concentrations ($[X_A, X_B] = \text{cm}^{-2}$), and let ν_A and ν_B be the corresponding average (and constant) concentrations, that is, the number of A and B atoms per unit area in the as-prepared surface alloy prior to the onset of a phase separation and electromigration. Then

$$\frac{X_A}{\nu_A} + \frac{X_B}{\nu_B} = C_A + C_B = 1, \quad (1)$$

where C_A and C_B are the dimensionless local time-dependent concentrations, or the local composition fractions.

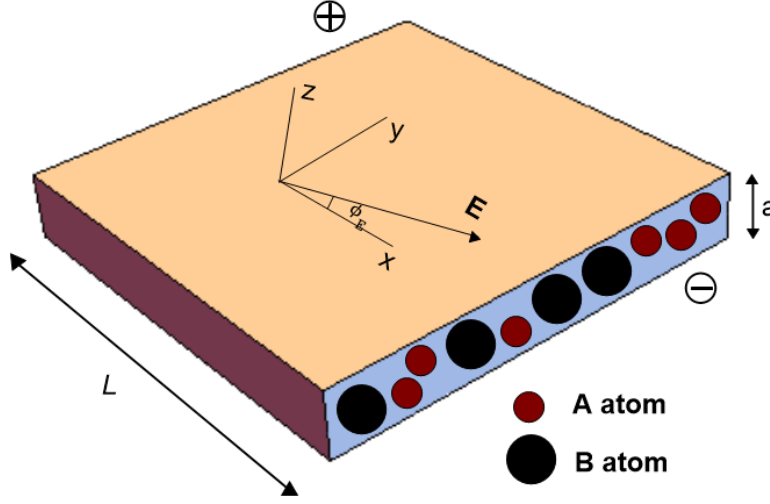


FIG. 1: Schematic representation of a single layer surface binary alloy subjected to an external electric field \mathbf{E} .

The diffusion equations read

$$\frac{\partial X_A}{\partial t} = -\nabla \cdot \mathbf{J}_A, \quad \frac{\partial X_B}{\partial t} = -\nabla \cdot \mathbf{J}_B, \quad (2)$$

where \mathbf{J}_A , \mathbf{J}_B are the components' fluxes measured in the laboratory reference frame, and $\nabla = (\partial_x, \partial_y)$. We are modeling the alloyed terrace as the two-dimensional (2D) diffusion couple, where diffusion is mediated by vacancies. Thus to ensure the mass conservation, according to the classical framework [19] one introduces the intrinsic (lattice) fluxes of the components, \mathbf{j}_A and \mathbf{j}_B , that are related to the fluxes in the laboratory frame via

$$\mathbf{j}_A = \mathbf{J}_A - \mathbf{v}X_A, \quad \mathbf{j}_B = \mathbf{J}_B - \mathbf{v}X_B, \quad (3)$$

where $\mathbf{v}(x, y, t)$ is the velocity field [7, 20]. The velocity field is measured in the laboratory frame and characterizes the velocity of the 2D surface lattice relative to the bulk, non-diffusing parts of the sample away from the interdiffusion area.

The conservation laws (2) then have the form:

$$\frac{\partial X_A}{\partial t} = -\nabla \cdot \mathbf{j}_A - \nabla \cdot (\mathbf{v}X_A), \quad \frac{\partial X_B}{\partial t} = -\nabla \cdot \mathbf{j}_B - \nabla \cdot (\mathbf{v}X_B). \quad (4)$$

Multiplying the first conservation law in Eq. (4) by $1/\nu_A$, the second conservation law by $1/\nu_B$, adding, and using Eq. (1) gives

$$\nabla \cdot \mathbf{v} = -\nabla \cdot \left(\frac{\mathbf{j}_A}{\nu_A} + \frac{\mathbf{j}_B}{\nu_B} \right). \quad (5)$$

The trivial solution of this equation for \mathbf{v} is assumed in the foregoing formulation:

$$\mathbf{v} = -\frac{\mathbf{j}_A}{\nu_A} - \frac{\mathbf{j}_B}{\nu_B}. \quad (6)$$

Eq. (6) states that the lattice moves in the direction opposite to the direction of the vector sum of the lattice fluxes \mathbf{j}_A and \mathbf{j}_B . It is expected that in practice the deviations from this rule are very small and thus in the first approximation they can be neglected ([7], p. 198). If the deviations cannot be neglected, the analysis becomes considerably more complicated [21]. Typically, the vectors \mathbf{j}_A/ν_A and \mathbf{j}_B/ν_B (which are analogous to $V_A\mathbf{j}_A$ and $V_B\mathbf{j}_B$ for the bulk alloy, where V_A and V_B are the partial molar volumes [21]) point in the opposite directions and their magnitudes are nearly equal, thus the lattice velocity is very small. Yet, for bulk three-dimensional alloys it can be measured in the interdiffusion/Kirkendall experiments. In this communication, the focus is not on modeling the probable Kirkendall effect in the binary surface alloy, but on demonstrating the surface atom transport effect of the applied electric current. Thus we are not concerned with the computation of Eq. (6), and it is presented only as part of the model formulation.

With $\nabla \cdot \mathbf{v}$ given by Eq. (5) and \mathbf{v} given by Eq. (6), it is seen that the expanded conservation laws

$$\frac{\partial X_A}{\partial t} = -\nabla \cdot \mathbf{j}_A - X_A \nabla \cdot \mathbf{v} - \mathbf{v} \cdot \nabla X_A, \quad \frac{\partial X_B}{\partial t} = -\nabla \cdot \mathbf{j}_B - X_B \nabla \cdot \mathbf{v} - \mathbf{v} \cdot \nabla X_B \quad (7)$$

are now explicitly formulated in terms of the lattice fluxes. We now proceed to the formulation of these fluxes.

According to the classical, irreversible thermodynamics-based phenomenological model of electromigration in metal alloys [5, 6],

$$\begin{aligned} \mathbf{j}_A &= -L_{AA} (\nabla [\mu_A - \mu_V] - q_A \mathbf{E}) - L_{AB} (\nabla [\mu_B - \mu_V] - q_B \mathbf{E}), \\ \mathbf{j}_B &= -L_{AB} (\nabla [\mu_A - \mu_V] - q_A \mathbf{E}) - L_{BB} (\nabla [\mu_B - \mu_V] - q_B \mathbf{E}). \end{aligned} \quad (8)$$

Here L_{AA} , L_{AB} , L_{BB} are the kinetic transport coefficients, μ_A , μ_B the chemical potentials of the components, μ_V the chemical potential of vacancies, and q_A , q_B the effective surface charges of the atom species A and B, respectively. The effective charges include the electrostatic and the electron-wind contributions, and are defined as

$$q_A = (Z_A^{(e)} + Z_A^{(w)}) e, \quad q_B = (Z_B^{(e)} + Z_B^{(w)}) e, \quad (9)$$

where $e < 0$ is the electron charge. Note that, since the sums $Z_i^{(e)} + Z_i^{(w)}$ of the effective ion valences may be positive or negative, q_A and q_B also may be positive or negative. When the magnitude of the electron-wind force is much larger than the magnitude of the electrostatic force, which is typical in surface electromigration phenomena [22, 23], the positive effective charge moves in the $-\mathbf{E}$ direction (equivalently, in the direction of the electron flow), that is, from the negatively charged anode to the positively charged cathode. Also note that due to formulating the diffusion equations in terms of the lattice fluxes, the kinetic transport coefficients are uniquely determined and their number is reduced from four to three, in other words, the off-diagonal coefficients are equal, $L_{BA} = L_{AB}$ [5, 6]. We further assume that the vacancy sources and sinks (such as the step edges) are sufficiently effective to keep μ_V constant, and also that the binding energies V-A and V-B are equal. Together, these assumptions allow to drop $\nabla \mu_V$ from Eqs. (8) [5].

The chemical potentials in Eq. (8) are due to alloy thermodynamics [26]:

$$\mu_A = \frac{C_B}{\nu_B} \left(\frac{\partial \gamma}{\partial C_A} - \frac{\partial \gamma}{\partial C_B} \right) - \frac{\epsilon a}{\nu_A} \nabla^2 C_A, \quad \mu_B = \frac{-C_A}{\nu_A} \left(\frac{\partial \gamma}{\partial C_A} - \frac{\partial \gamma}{\partial C_B} \right) - \frac{\epsilon a}{\nu_B} \nabla^2 C_B, \quad (10)$$

where γ is the free energy, a the lattice spacing, and ϵ the Cahn-Hilliard gradient energy coefficient.

The free energy is chosen as [27, 28]:

$$\gamma = \gamma_A C_A + \gamma_B C_B + kT\nu (C_A \ln C_A + C_B \ln C_B + H C_A C_B), \quad (11)$$

where it is assumed $\nu_A = \nu_B = \nu$, γ_A (γ_B) is the surface energy of atomically thin surface layer that is composed of A (B) atoms, $kT\nu$ the alloy entropy, and the dimensionless number $H = \alpha_{int}/kT\nu$ measures the bond strength relative to the thermal energy kT . Here α_{int} is the enthalpy. The terms in the parenthesis are the regular solution model.

Apart from the constant matrix \mathbf{W} , which will be introduced shortly, the kinetic transport coefficients have the forms derived from Manning's model of diffusion in nondilute alloys [24, 25]:

$$\begin{aligned} L_{AA} &= \Gamma_B \Gamma C_A \frac{\lambda a^2 \nu}{kT} \left(1 - \frac{2\Gamma C_B}{\psi} \right) \mathbf{W}, \quad L_{AB} = \Gamma_B \Gamma C_A C_B \frac{2\lambda a^2 \nu}{kT\psi} \mathbf{W}, \\ L_{BB} &= \Gamma_B C_B \frac{\lambda a^2 \nu}{kT} \left(1 - \frac{2C_A}{\psi} \right) \mathbf{W}, \end{aligned} \quad (12)$$

where the dimensionless ψ is given by

$$\psi = \frac{1}{2} (M_0 + 2) (\Gamma C_A + C_B) - \Gamma - 1 + 2 (C_A + \Gamma C_B) + \sqrt{\left[\frac{1}{2} (M_0 + 2) (\Gamma C_A + C_B) - \Gamma - 1 \right]^2 + 2M_0\Gamma}. \quad (13)$$

In Eqs. (12) and (13), $\Gamma = \Gamma_A/\Gamma_B$, Γ_A and Γ_B are the jump frequencies of species A and B, respectively, $M_0 = 2f_0/(1-f_0)$, f_0 and λ are the tracer correlation factor and the dimensionless geometric factor for fcc lattice, respectively, and \mathbf{W} the diagonal tensor,

$$\mathbf{W} = \begin{pmatrix} 1 & 0 \\ 0 & \Lambda \end{pmatrix}, \quad (14)$$

where the dimensionless Λ measures the difference in the diffusion strength along the x and y axes. Specifically, if we let D_x and D_y be the diffusivities along the x and y axes, respectively, then $D_y = \Lambda D_x$. Thus the multiplication of the kinetic transport coefficients by \mathbf{W} allows to account for the possible directional diffusional anisotropy in the xy -plane. When $\Lambda = 1$, $\mathbf{W} = \mathbf{I}$, where \mathbf{I} is the identity tensor, and the diffusion becomes isotropic.

Equations (1), (5)-(8), (10)-(14) constitute our dimensional model, with $\nu_A = \nu_B = \nu$ in Eq. (10). To render this model dimensionless, we chose a as the length scale and $kT\nu/(\gamma_B\lambda\Gamma_B)$ as the time scale. After elimination of C_A using Eq. (1), we arrive to the final dimensionless model for the spatio-temporal dynamics of the concentration of B atoms:

$$\frac{\partial C_B}{\partial t} = (1 - C_B) (\nabla \cdot \Sigma_A - F_e \nabla \cdot \Omega_A) - C_B (\nabla \cdot \Sigma_B - F_e \nabla \cdot \Omega_B) - (\Sigma_A + \Sigma_B - F_e \Omega_A - F_e \Omega_B) \cdot \nabla C_B, \quad (15)$$

$$\Sigma_A = \bar{L}_{AA} \nabla_\Lambda \mu_A + \bar{L}_{AB} \nabla_\Lambda \mu_B, \quad \Sigma_B = \bar{L}_{AB} \nabla_\Lambda \mu_A + \bar{L}_{BB} \nabla_\Lambda \mu_B, \quad (16)$$

$$\Omega_A = [Q\bar{L}_{AA} + \bar{L}_{AB}] \begin{pmatrix} \cos \phi_E \\ \Lambda \sin \phi_E \end{pmatrix}, \quad \Omega_B = [\bar{L}_{AB} + \bar{L}_{BB}] \begin{pmatrix} \cos \phi_E \\ \Lambda \sin \phi_E \end{pmatrix}, \quad (17)$$

$$\bar{L}_{AA} = \Gamma (1 - C_B) \left(1 - \frac{2\Gamma C_B}{\psi} \right), \quad \bar{L}_{AB} = \frac{2}{\psi} \Gamma C_B (1 - C_B), \quad \bar{L}_{BB} = C_B \left(1 - \frac{2(1 - C_B)}{\psi} \right), \quad (18)$$

$$\mu_A = -C_B \frac{\partial \gamma}{\partial C_B} + \xi \nabla^2 C_B, \quad \mu_B = (1 - C_B) \frac{\partial \gamma}{\partial C_B} - \xi \nabla^2 C_B, \quad (19)$$

$$\gamma = G(1 - C_B) + C_B + N[(1 - C_B) \ln(1 - C_B) + C_B \ln C_B + H C_B (1 - C_B)], \quad (20)$$

$$\psi = \frac{1}{2} (M_0 + 2) (\Gamma (1 - C_B) + C_B) - \Gamma - 1 + 2((1 - C_B) + \Gamma C_B) + \sqrt{\left[\frac{1}{2} (M_0 + 2) (\Gamma (1 - C_B) + C_B) - \Gamma - 1 \right]^2 + 2M_0\Gamma}, \quad (21)$$

$$\nabla_\Lambda = \begin{pmatrix} \partial_x \\ \Lambda \partial_y \end{pmatrix}. \quad (22)$$

Here, ∇_Λ is the anisotropic gradient operator, which reduces to the ∇ operator when diffusion is isotropic. The fluxes Σ_A and Σ_B are due to the gradients of the chemical potentials, whereas the fluxes Ω_A and Ω_B are the electromigration fluxes. Since the anisotropy matrix \mathbf{W} enters the three kinetic transport coefficients in Eqs. (8), all fluxes are anisotropic either due to presence of ∇_Λ , or due to presence of the column vector $\begin{pmatrix} \cos \phi_E \\ \Lambda \sin \phi_E \end{pmatrix}$. Also, \bar{L}_{AA} , \bar{L}_{AB} and \bar{L}_{BB} are the dimensionless, and now isotropic, kinetic transport coefficients. We point out for the interested reader that Eq. (15) does not have a divergence form that is expected for a standard diffusion equation. Due to the terms $-\mathbf{v} \cdot \nabla X_A$ and $-\mathbf{v} \cdot \nabla X_B$ in Eqs. (7), this equation contains the convective terms $-(\Sigma_A + \Sigma_B - F_e \Omega_A - F_e \Omega_B) \cdot \nabla C_B$.

Physical parameter	Typical value	Dimensionless parameter	Typical value
L	10^{-5} cm (100 nm) [1]	Γ	2
a	3.38×10^{-8} cm (0.338 nm)	Λ	1
$\nu = a^{-2}$	8×10^{14} cm $^{-2}$	H	2.2
λ	1/6 [24]	M_0	7.153
f_0	0.7815 [24]	ϕ_E	π
T	400 K [3]	G	1
q_A, q_B	$20 e = 10^{-8}$ statC [22, 23]	N	0.02
V	5×10^{-5} V	ξ	0.16
α_{int}	100 erg/cm 2	Q	1
γ_A, γ_B	2.2×10^3 erg/cm 2 [29]	F_e	7.7×10^{-4}
ϵ	1.2×10^{-5} erg/cm [30]		

TABLE I: Physical and dimensionless parameters. a , γ_A , and γ_B correspond to fcc CuPd alloy, other physical parameters are the generic values typical to most binary surface alloys. ($a = 2R_{Pd}$, where $R_{Pd} = 0.169$ nm is the calculated radius of a Pd atom [31].)

Eqs. (15)-(22) contain ten dimensionless parameters. Parameters Γ , Λ , H , M_0 , ϕ_E were introduced above. Note, when $H > 2$, the graph of γ is a double-well curve, which results in the spinodal decomposition of the alloy. The condition $H > 2$ is equivalent to $T < T_c = \alpha_{int}/2k\nu$ [28], and for the parameters in Table I, $T_c = 450$ K. Other parameters are: $G = \gamma_A/\gamma_B$, the ratio of the surface energies of the components; $N = kT\nu/\gamma_B$: the alloy entropy; $\xi = \epsilon/a\gamma_B$: the Cahn-Hilliard gradient energy coefficient; $Q = q_A/q_B > 0$: the ratio of the effective charges; $F_e = q_B a \nu V / L \gamma_B > 0$: the electric field strength.

The dimensionless kinetic transport coefficients are plotted in Fig. 2. Note that at $\Gamma \rightarrow 0$, meaning $\Gamma_B \gg \Gamma_A$, only \bar{L}_{BB} is not zero, thus A atoms are immobile. And at $\Gamma \rightarrow \infty$, meaning $\Gamma_A \gg \Gamma_B$, \bar{L}_{BB} and \bar{L}_{AB} are negligible in comparison to \bar{L}_{AA} , thus B atoms are effectively immobile. At $\Gamma = 1$ ($\Gamma_A = \Gamma_B$), $\bar{L}_{AA} = \bar{L}_{BB}$.

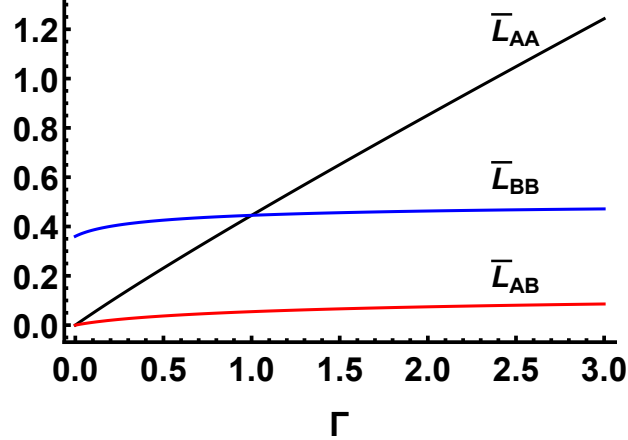


FIG. 2: Kinetic transport coefficients \bar{L}_{AA} , \bar{L}_{AB} and \bar{L}_{BB} at $C_B = 0.5$. At $\Gamma = 2$ (A is fast diffuser), $\bar{L}_{AA} = 0.851$, $\bar{L}_{BB} = 0.463$, $\bar{L}_{AB} = 0.074$. At $\Gamma = 0.2$ (B is fast diffuser), $\bar{L}_{AA} = 0.096$, $\bar{L}_{BB} = 0.4$, $\bar{L}_{AB} = 0.02$. These values mildly change as C_B is varied, and they are provided (only for comparison of the magnitudes, not for computation), since $\Gamma = 2, 0.2$ is adopted in section III.

III. COMPUTATIONAL RESULTS

Computations of Eq. (15) are performed on the square, bi-periodic domain of the size 550 lattice spacings. The initial condition $C_B(x, y, 0)$ is chosen in the form of a local composition inhomogeneity positioned at the square

center; see Fig. 3(a). Within this initial square cluster, the concentration of B atoms is increased to 60% (see the color bar). This is 10% higher than outside of the cluster, where the species A and B have equal concentrations, that is, 50%A/50%B.

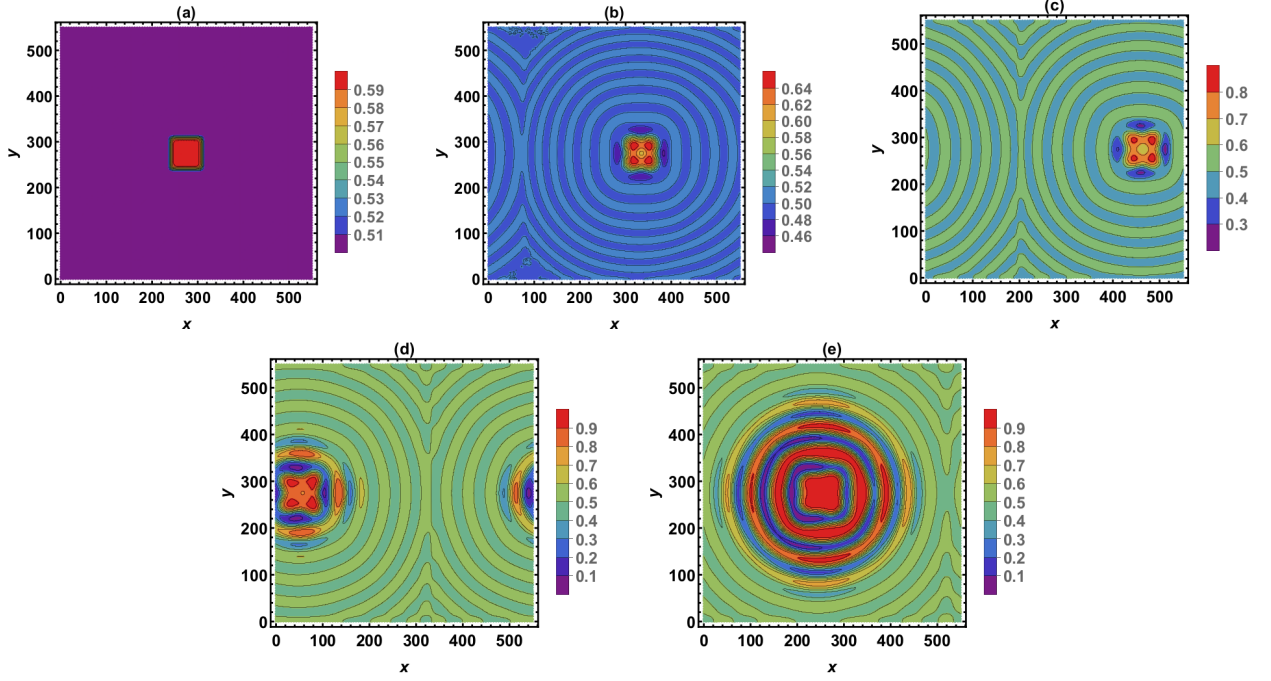


FIG. 3: C_B at (a): $t = 0$ (the initial condition), (b): $t = 5 \times 10^4$, (c): $t = 1.6 \times 10^5$, (d): $t = 2.8 \times 10^5$, (e): $t = 4.5 \times 10^5$. All parameters as in Table I.

Panels (b)-(e) of Fig. 3 show the transport (drift) of the cluster due to the electromigration effect caused by the electric field \mathbf{E} in the 180° direction (see Fig. 1). The dimensionless parameters are taken from Table I. After drifting across the half of the computational domain, the cluster re-emerges at the left boundary of the domain due to the periodic boundary condition. By $t = 4.5 \times 10^5$ the center of the cluster covered the distance of approximately 525 lattice spacings. We estimate value of Γ_B from the Arrhenius-type expression $\Gamma_B = \sigma \exp(-E_a/kT)$, where $\sigma = 10^{13} \div 10^{14} \text{Hz}$ is the attempt frequency and $E_a \simeq 1 \text{eV}$ the activation energy [32]. This gives $\Gamma_B = 4 \div 40 \text{Hz}$ and translates into the speed of $0.04 \div 0.4$ lattice spacings/second. As the cluster drifts, it collects B atoms from the surface layer due to developing phase separation instability; close to the end of the run, the cluster's composition is 100% B phase, see the color bars in Fig. 3(d,e). The cluster keeps its initial compact shape, but the development of the instability, which takes place independently of, and alongside with the drift, results in the emergence of B-rich concentric rings that propagate away from the cluster. Visually, this situation looks like the surface water waves after a pebble is dropped in the pond.

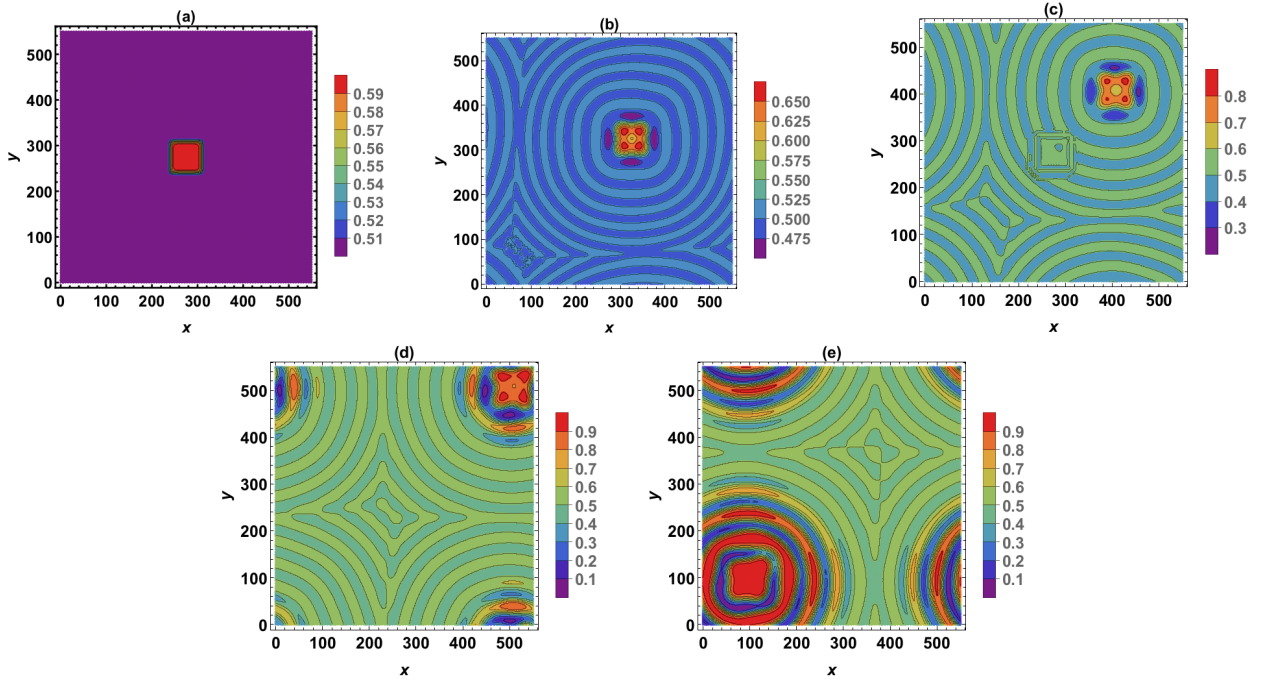


FIG. 4: C_B at (a): $t = 0$ (the initial condition), (b): $t = 5 \times 10^4$, (c): $t = 1.6 \times 10^5$, (d): $t = 2.8 \times 10^5$, (e): $t = 4.5 \times 10^5$. $\phi_E = 3\pi/4$, other parameters as in Table I.

In Fig. 4 the direction of the electric field, and of the current, is 225° , and all other parameters are still as in Table I. The cluster is shown at the same times as the one in Fig. 3. The change in the electric field direction results in the cluster drifting along the square's diagonal with the same speed and other features seen in Fig. 3. From Figures 3 and 4 it is clear that the electromigration very reliably transports the cluster carrying the effective positive charge, across the terrace in the direction that is the opposite to the direction of the current.

In the remaining computations (except the results shown in Fig. 8) we fix the electric field direction to 180° , as in Fig. 3, and study the effects of other parameters.

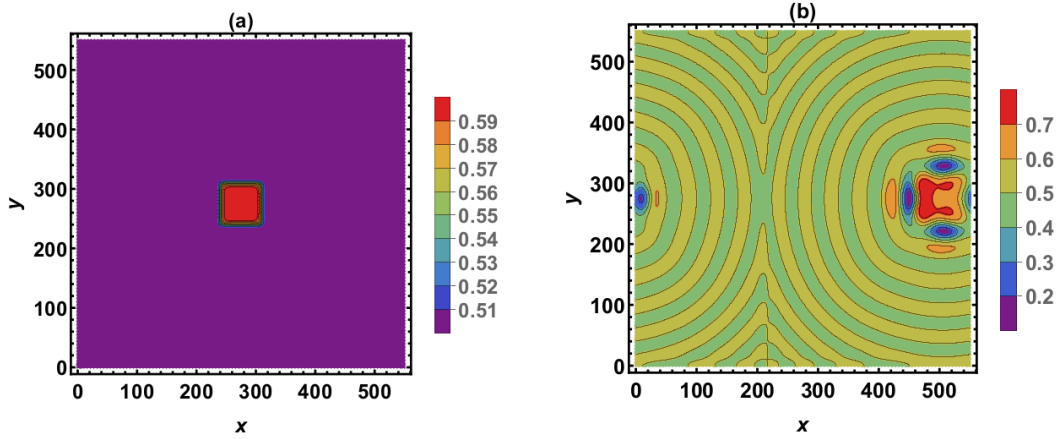


FIG. 5: C_B at (a): $t = 0$ (the initial condition), (b): $t = 5 \times 10^5$. $\Gamma = 0.2$, other parameters as in Table I.

Next, Fig. 5 shows the effect of varying the parameter Γ . As Γ is decreased ten-fold compared to Table I value, the speed of the cluster decreased roughly by the factor of three, compare to Fig. 3(c). Since Γ_B is kept constant at, say, 40Hz (notice that Γ_B enters only the time scale, which has not changed), the stated decrease of Γ is due to the ten-fold decrease of Γ_A . Thus the slow-down of the drift is attributed to the smaller hop frequency of A atoms, which resulted in the decrease of the kinetic transport coefficients, see Fig. 2 and its caption. Also note that despite the slower cluster drift, its enrichment by B atoms, seen in Fig. 5(b), is less efficient than in Fig. 3(c) - apparently, due to slower outflow of A atoms from the cluster and therefore their slower replacement by B atoms.

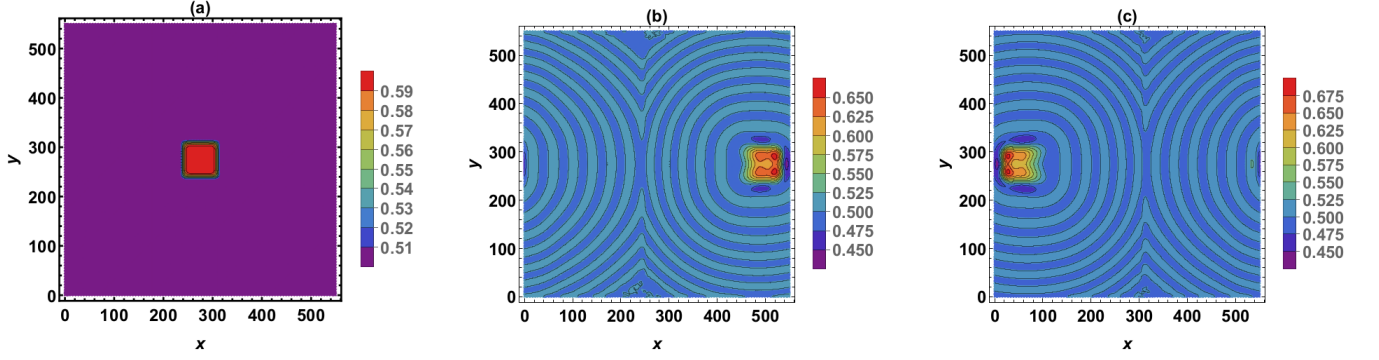


FIG. 6: C_B at (a): $t = 0$ (the initial condition), (b): $t = 5 \times 10^4$, $q_A = 5q_B > 0$ ($Q = 5$), other parameters as in Table I, (c): $t = 6 \times 10^4$, $q_A = -5q_B < 0$ ($Q = -5$), other parameters as in Table I.

In Fig. 6(b) it is seen that larger (but still positive) effective charge of A atoms ($q_A \rightarrow 5q_A$) speeds up the drift, again roughly by the factor of three, compare to Fig. 3(c). Upon nearly reaching the right boundary of the computational domain (the drift distance 225 lattice spacings), the initial composition of the cluster experienced the change of only 5%. As can be expected, changing not only the magnitude, but also the sign of q_A results in the reversal of the drift direction (Fig. 6(c)), the speed and other features are unchanged from Fig. 6(b).

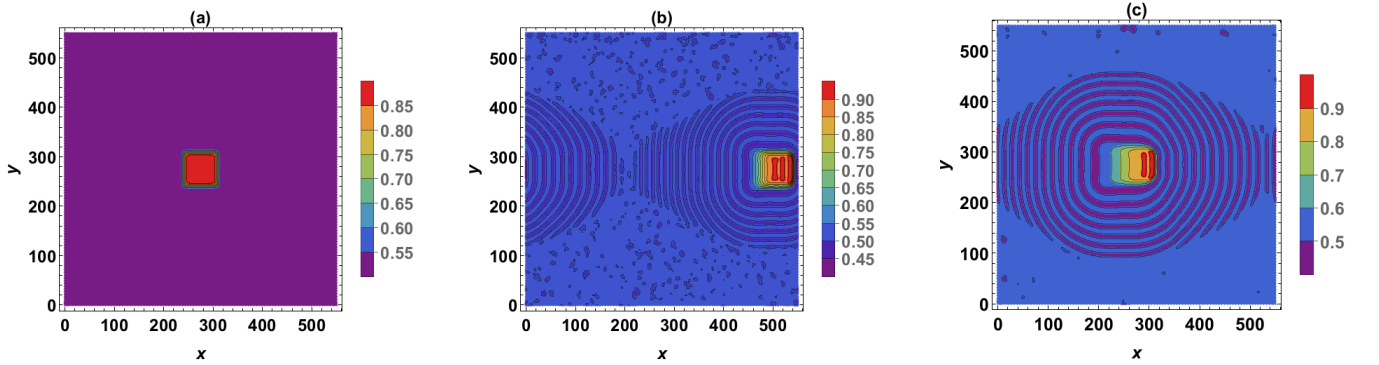


FIG. 7: C_B at (a): $t = 0$ (the initial condition), (b): $t = 1.9 \times 10^3$, (c): $t = 4.5 \times 10^3$. $V = 5 \times 10^{-3}V$, other parameters as in Table I.

For Fig. 7 the applied voltage in Table I is increased 100 times. The drift speed increased by the same factor (again compare to Fig. 3(c)). Unless $G > 1$, at such high drift speed there is insufficient time for the efficient phase separation to develop over drift distance of hundreds of lattice spacings. However, suppose that the initial cluster's composition is already highly B-rich (say, 90% B phase as in Fig 7(a)). Then this initial condition is transported by the electromigration over very long distances, and the purity slightly improves in the process (Fig. 7(b,c)). Note that after drifting over the full width of the domain, nearly all A atoms had been expunged from the cluster. If $\gamma_A > \gamma_B$ ($G > 1$) the phase separation is still efficient over the short time scale of crossing the terrace, and the initial cluster with only 10% higher concentration of B atoms reaches 100% B content by the time the crossing is completed. The latter simulation is not shown, as it looks very similar to Fig. 7(b,c).

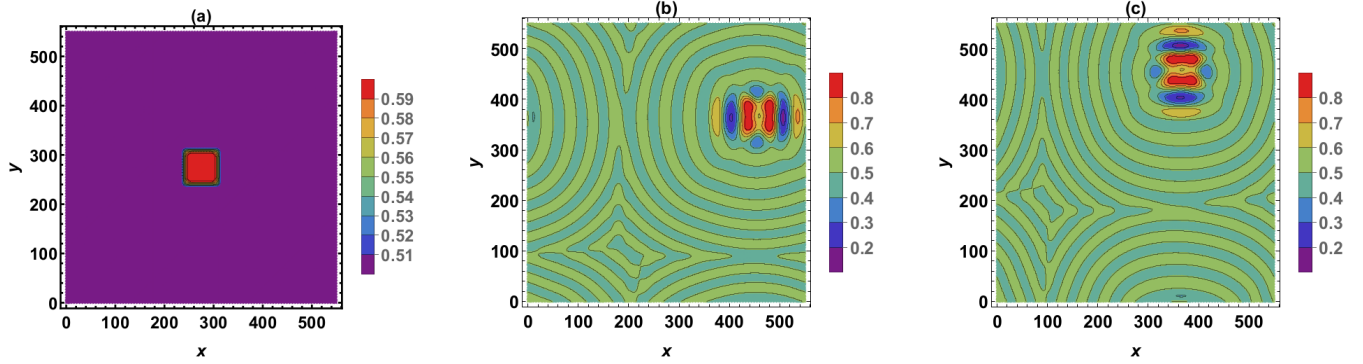


FIG. 8: C_B at (a): $t = 0$ (the initial condition), (b): $t = 2.2 \times 10^5$, $\Lambda = 0.5$, $\phi_E = 3\pi/4$, other parameters as in Table I, (c): $t = 1.1 \times 10^5$, $\Lambda = 2$, $\phi_E = 3\pi/4$, other parameters as in Table I.

Lastly, in Fig. 8 we clarify the impact of the diffusion anisotropy. When present[33], strong anisotropy has the detrimental effect both on the target direction of the drift and on the compactness of the cluster. This is clear from Fig. 8(b,c). At $\Lambda = 0.5$ (Fig. 8(b)), the diffusion in the x -direction is twice as strong as in the y -direction, which results in some cluster smearing along the x -direction and the simultaneous straying away, by about 10° , from the path along the square's diagonal. At $\Lambda = 2$, when the diffusion in the y -direction is twice as strong as in the x -direction, the similar effects can be seen with respect to the y -direction.

To summarize, we suggested harnessing a phase-separation instability and surface electromigration for long-range transport of A or B atom clusters in the topmost surface layer of a surface binary alloy. Computation demonstrates that the transport is robust across a wide range of the control parameters.

-
- [1] R. van Gastel, E. Somfai, S.B. van Albada, W. van Saarloos, and J.W.M. Frenken, “Nothing moves a surface: Vacancy-mediated surface diffusion”, *Phys. Rev. Lett.* **86**, 1562 (2001).
 - [2] M.L. Grant, B.S. Swartzentruber, N.C. Bartelt, and J.B. Hannon, “Diffusion kinetics in the Pd/Cu(001) surface alloy”, *Phys. Rev. Lett.* **86**, 4588 (2001).
 - [3] M.L. Anderson, M.J. D’Amato, P.J. Feibelman, and B.S. Swartzentruber, “Vacancy-mediated and exchange diffusion in a Pb/Cu(111) surface alloy: Concurrent diffusion on two length scales”, *Phys. Rev. Lett.* **90**, 126102 (2003).
 - [4] R. van Gastel, E. Somfai, W. van Saarloos, and J.W.M. Frenken, “A giant atomic slide-puzzle”, *Nature* **408**, 665 (2000).
 - [5] H.B. Huntington, Ch. 6: Electromigration in metals, in: *Diffusion in Solids: Recent Developments*, Ed. A.S. Nowick, Academic Press, 1975.
 - [6] P.S. Ho and T. Kwok, “Electromigration in metals”, *Rep. Prog. Phys.* **52**, 301-348 (1989).
 - [7] H. Mehrer, *Diffusion in solids*. Springer (2007).
 - [8] M. Khennner, “Electromigration-guided composition patterns in thin alloy films: a computational study”, *Surf. Sci.* **698**, 121611 (2020).
 - [9] S. Curiotto, P. Muller, A. El-Barraj, F. Cheynis, O. Pierre-Louis, and F. Leroy, “2D nanostructure motion on anisotropic surfaces controlled by electromigration”, *Appl. Surf. Sci.* **469**, 463-470 (2019).
 - [10] P. Kuhn, J. Krug, F. Hausser, and A. Voigt, “Complex Shape Evolution of Electromigration-Driven Single-Layer Islands”, *Phys. Rev. Lett.* **94**, 166105 (2005).
 - [11] D. Dasgupta and D. Maroudas, “Surface nanopatterning from current-driven assembly of single-layer epitaxial islands”, *Appl. Phys. Lett.* **103**, 181602 (2013).
 - [12] D. Dasgupta, A. Kumar, and D. Maroudas, “Analysis of current-driven oscillatory dynamics of single-layer homoepitaxial islands on crystalline conducting substrates”, *Surf. Sci.* **669**, 25 (2018).
 - [13] A. Kumar, D. Dasgupta, C. Dimitrakopoulos, and D. Maroudas, “Current-driven nanowire formation on surfaces of crystalline conducting substrates”, *Appl. Phys. Lett.* **108**, 193109 (2016).
 - [14] D. Solenov and K.A. Velizhanin, “Adsorbate transport on graphene by electromigration”, *Phys. Rev. Lett.* **109**, 095504 (2012).
 - [15] C.-H. Chiu, Z. Huang, and C. T. Poh, “Formation of nanoislands by the electromolding self-organization process”, *Phys. Rev. B* **73**, 193409 (2006).
 - [16] J.W. Cahn and J. Hilliard, “Free energy of a nonuniform system. Interfacial free energy”, *J. Chem. Phys.* **28**, 258-267 (1958).
 - [17] J.W. Cahn, “On spinodal decomposition,”, *Acta Metall.* **9**, 795-801 (1961).
 - [18] Ge-Bo Pan and W. Freyland, “In situ STM investigation of spinodal decomposition and surface alloying during underpotential deposition of Cd on Au(111) from an ionic liquid”, *Phys. Chem. Chem. Phys.* **9**, 3286-3290 (2007).

- [19] L.S. Darken, “Diffusion, mobility, and their interrelation through free energy in binary metallic systems”, *Transactions of the Metall. Soc. of AIME* **175**, 184-201 (1948).
- [20] A.M. Gusak, “Nonequilibrium vacancies and diffusion-controlled processes at nanolevel”, in: *Diffusion-controlled solid state reactions: In Alloys, Thin Films and Nanosystems*. Wiley-VCH, 2011.
- [21] W.J. Boettinger, J.E. Guyer, C.E. Campbell, and G.B. McFadden, “Computation of the Kirkendall velocity and displacement fields in a one-dimensional binary diffusion couple with a moving interface”, *Proc. Roy. Soc.: Math., Phys. and Eng. Sci.* **463**, 3347-3373 (2007).
- [22] P.J. Rous, T.L. Einstein, and E.D. Williams, “Theory of surface electromigration on metals: application to self-electromigration on Cu(111)”, *Surf. Sci.* **315**, L995-L1002 (1994).
- [23] K.H. Bevan, H. Guo, E.D. Williams, and Z. Zhang, “First-principles quantum transport theory of the enhanced wind force driving electromigration on Ag(111)”, *Phys. Rev. B* **81**, 235416 (2010).
- [24] J.R. Manning, “Correlation factors for diffusion in nondilute alloys”, *Phys. Rev. B* **4**, 1111 (1971).
- [25] H. Ribera, B.R. Wetton, and T.G. Myers, “Mathematical model for substitutional binary diffusion in solids”, arXiv:1911.07359v1 (2019).
- [26] Q. Zhang, P.W. Voorhees, and S.H. Davis, “Mechanisms of surface alloy segregation on faceted core-shell nanowire growth”, *J. Mech. Phys. Solids* **100**, 21-44 (2017).
- [27] A.V. Ruban, H.L. Skriver, and J.K. Norskov, “Local equilibrium properties of metallic surface alloys”, in: *The Chemical Physics of Solid Surfaces*, Ed.: D.P. Woodruff, vol. 10, Elsevier (2002).
- [28] W. Lu and D. Kim, “Engineering nanophase self-assembly with elastic field”, *Acta Mater.* **53**, 3689 (2005).
- [29] L. Vitos, A.V. Ruban, H.L. Skriver, and J. Kolla, “The surface energy of metals”, *Surf. Sci.* **411**, 186-202 (1998).
- [30] J.J. Hoyt, “Molecular dynamics study of equilibrium concentration profiles and the gradient energy coefficient in Cu-Pb nanodroplets”, *Phys. Rev. B* **76**, 094102 (2007).
- [31] E. Clementi, D.L. Raimondi, and W.P. Reinhardt, “Atomic Screening Constants from SCF Functions. II. Atoms with 37 to 86 Electrons”, *J. Chem. Phys.* **47**, 1300 (1967).
- [32] E. Bussmann, I. Ermanoski, P. J. Feibelman, N. C. Bartelt, and G. L. Kellogg, “Buried Pd slows self-diffusion on Cu(001)”, *Phys. Rev. B* **84**, 245440 (2011).
- [33] Ref. [2] provides the ratio close to 0.25 of the number of the diagonal hops over the distance $\sqrt{2}a$ to the number of hops over the distance a along the x or y direction. This seems to indicate that diffusion anisotropy is typically manifested in vacancy-mediated surface diffusion.